(12) **LEVEL** II AD-E000490

NRL Memorandum Report 4247

AD-E000490

ADA086999

Gas Channel Formation Studies Including Real-Air Thermodynamic Properties

Selig Kainer and Martin Lampe

Plasma Theory Branch
Plasma Physics Division

June 26, 1980

DTIC
SELECTED
JUL 2 3 1980
B

NAVAL RESEARCH LABORATORY
Washington, D.C.

DDC FILE COPY

80 7 11 017

REPORT DOCUMENTATION PAGE	READ INSTRUCTIONS BEFORE COMPLETING FORM

1. REPORT NUMBER	2. GOVT ACCESSION NO.	3. RECIPIENT'S CATALOG NUMBER
NRL Memorandum Report 4247	AD-A86 999	

4. TITLE *(and Subtitle)*	5. TYPE OF REPORT & PERIOD COVERED
GAS CHANNEL FORMATION STUDIES INCLUDING REAL-AIR THERMODYNAMIC PROPERTIES.	Interim report on a continuing NRL problem.
	6. PERFORMING ORG. REPORT NUMBER

7. AUTHOR(s)	8. CONTRACT OR GRANT NUMBER(s)
J. Kainer and M. Lampe	ARPA Order-3718

9. PERFORMING ORGANIZATION NAME AND ADDRESS	10. PROGRAM ELEMENT, PROJECT, TASK AREA & WORK UNIT NUMBERS
Naval Research Laboratory Washington, D.C. 20375	61101E; 67-0900-0-0

11. CONTROLLING OFFICE NAME AND ADDRESS	12. REPORT DATE
Defense Advanced Research Projects Agency Arlington, VA 22090	June , 1980
	13. NUMBER OF PAGES
	29

14. MONITORING AGENCY NAME & ADDRESS *(if different from Controlling Office)*	15. SECURITY CLASS. *(of this report)*
Naval Surface Weapons Center Silver Spring, MD 20910	UNCLASSIFIED
	15a. DECLASSIFICATION/DOWNGRADING SCHEDULE

16. DISTRIBUTION STATEMENT *(of this Report)*

Approved for public release; distribution unlimited.

NRL-MR-4247

17. DISTRIBUTION STATEMENT *(of the abstract entered in Block 20, if different from Report)*

18. SUPPLEMENTARY NOTES

This research was sponsored by Defense Advanced Research Projects Agency (DoD) ARPA Order No. 3718, and Naval Surface Weapons Center under Contract N60921-80-WR-W0190.

19. KEY WORDS *(Continue on reverse side if necessary and identify by block number)*

Gas channel formation	Charged particle beam
Hole boring	Real-air thermodynamics
Hydrodynamics	

20. ABSTRACT *(Continue on reverse side if necessary and identify by block number)*

Real-air thermodynamic properties are included in studies of reduced density channel formation by expansion of a heated cylinder of air. A model for the density profile at late times, previously given for a polytropic ideal gas, is extended to the present case. It is shown that a relation between pressure P, density ρ, and specific energy ϵ, of the form properties. The variation of f with ϵ, i.e. of specific heat with temperature, can strongly modify the initial pressure profile associated with a given energy density profile. The effects of real-gas thermodynamics during the hydrodynamic expansion, on the other hand, are rather weak.

DD FORM 1473 JAN 73   EDITION OF 1 NOV 68 IS OBSOLETE
S/N 0102-LF-014-6601

CONTENTS

ACCESSION for

NTIS	White Section	✓
DDC	Buff Section	☐
UNANNOUNCED		☐
JUSTIFICATION		

BY
DISTRIBUTION/AVAILABILITY CODES

| Dist. | AVAIL. and/or SPECIAL | |
| A | | |

GAS CHANNEL FORMATION STUDIES INCLUDING
REAL-AIR THERMODYNAMIC PROPERTIES

1. Introduction

Hot reduced-density channels can be formed in gases by methods such
as exploding wires[1], lasers[2], pulsed electrical discharges[3], or charged
particle beams[4]. In many cases, the heating occurs very rapidly com-
pared to the hydrodynamic response time of the gas (the sound transit
time over the channel radius), and can thus be treated as instantaneous.
Furthermore, cooling due to heat conduction and radiation is slow, for
many applications, and can be neglected in treating the hydrodynamic
response. Under these conditions, channel formation is a one-
dimensional hydrodynamic process which departs from adiabaticity only
because of the occurrence of shock waves. Analytic solutions for this
process, in the form of self-similar blast waves[5], are appropriate at
very high initial overpressure, but in the range of primary interest
to us, with overpressure less than a hundred times ambient, it is
necessary to run one-dimensional fluid codes to calculate the time
evolution of the overheated channel.

We have previously reported[6] fluid code studies of this process
for the case in which the heating source has a very smoothly rounded
radial profile, e.g. the Bennett profile appropriate for a self-pinched
electron beam. In this case, we found that the channel formation
process went through the following stages: (i) Initially, the gas is

at uniform density, but with an overpressure profile corresponding to the source heating profile. (ii) A rarefaction wave reduces the gas density within the heating source radius. (iii) An outgoing shock wave forms near the point of steepest slope of the initial overpressure profile, and leads to expansion of the gas over a channel broader than the source radius. (iv) When the shock detaches from the channel, the entire channel is left at a pressure of about 85-90% of ambient. (v) The channel slowly returns to ambient pressure, with a density rise of about 10% and no further shock formation. (vi) The final density profile is determined strictly by adiabatic expansion in the central channel, but the density is further depressed in the radial wings by the entropy increase attendant upon shock heating. Under these conditions, we gave an analytic formulation of the density profile at late times, when pressure balance has been restored.[6] This formulation depended on the "polytropic" assumption that the ratio γ of the specific heat c_p (at constant pressure) and c_v (at constant volume) is a constant, which we usually took to be $\gamma \equiv c_p/c_v = 1.4$, characteristic of a diatomic gas at moderate temperature. For simplicity and comparability, we used the same assumption in our fluid code runs.

In a real diatomic gas, γ depends on both temperature T and density ρ, and decreases from ~ 1.4 at room temperature to less than 1.2 at T > 3000°K. The purpose of the present rate is to include this variation in the analytic formulation, which becomes possible because a generalized form of γ can be expressed as a function of specific energy ε, with practically no further dependence on ρ. We also show

2

the effect of including real gas thermodynamics in the fluid code runs.

In another previous report[7], we have shown that the hydrodynamic evolution becomes somewhat more complex, with ringing of the channel and sometimes multiple shocks occurring, if the radial profile of the heating source is squarer in shape, or has discontinuities. These complications are treated only in passing in the present note.

In Sec. 2, we give a convenient summary and formulation of the real gas thermodynamic properties required. In Sec. 3, we include these properties in a semi-analytic model of the density profile at late time. In Sec. 4, we compare the results of the model with numerical studies performed on the one-dimensional (cylindrical) Eulerian flux-corrected transport fluid code FAST1D.[6-9]

2. Real Gas Thermodynamics

A particularly convenient way of specifying the thermodynamic properties of a real gas is by means of a constitutive equation,

$$P/\rho = \epsilon f(\epsilon, \rho), \tag{1}$$

supplemented by an ideal gas equation of state,

$$P/\rho = (k_B/M)\left[1 + \alpha(\epsilon, \rho)\right]T, \tag{2}$$

where P is pressure, ρ is density, ϵ is specific energy (thermal plus internal, but excluding any macroscopic kinetic energy), T is temperature, k_B is Boltzmann's constant, M is the molecular mass, and f and α are functions that characterize the gas species. The quantity α measures the degree of dissociation and ionization; it is unity for the undissociated, unionized state, and is equal in general to the mean number of dissociated atoms, ions and electrons per molecule. The quantity f is a generalization of the adiabatic index γ, defined by

$$\gamma \equiv c_p/c_v, \tag{3}$$

for the case in which the specific heats c_p (at constant pressure) and c_v (at constant volume) are constant. In this case,

$$f(\epsilon, \rho) = \gamma - 1, \tag{4}$$

and the adiabatic relations

$$P/\rho^\gamma = \text{const}, \tag{5}$$

$$\epsilon/\rho^{\gamma-1} = \text{const} \tag{6}$$

can be used to characterize adiabatic flows.

In a diatomic gas such as air, $f(\varepsilon,\rho)$ ranges from 2/3 at cryogenic temperatures where ε consists entirely of translational thermal energy, to 2/5 at room temperature, where rotational states are fully excited, to 2/7 at T $\sim$ 3000°K, where vibrational states are fully excited. Up to this point, $f(\varepsilon,\rho)$ is quite independent of density. At still higher temperatures, $f(\varepsilon,\rho)$ decreases further as electronic excitation, dissociation, and ionization begin to contribute to ε. Since the latter two processes change the number of particles, they lead to a ρ dependence of f. However the particular form (1) was chosen because this ρ dependence remains minimal, even in this regime. This point is illustrated in Fig. 1, where $f(\varepsilon,\rho)$, taken from the tabulated values of Ref. 10, is plotted for air at a variety of densities, at temperatures up to $\sim$ 10,000°K, and it is seen that varying ρ over a wide range changes $f(\varepsilon,\rho)$ no more than 10%. Consequently, we can regard f as a function of ε alone,

$$f(\varepsilon,\rho) = f(\varepsilon), \tag{7}$$

which leads to considerable simplification in our analysis. If f were regarded as a function of T and ρ, or if a relation were written between ε and T, the ρ dependence would be much stronger. A second advantage of the formulation used in Eqs. (1) and (2) is that, for most purposes, we do not need to know T, so that only Eq. (1) is used.

3.   Density Profile at Late Times

The first law of thermodynamics,

$$T ds = d\epsilon + P d\rho^{-1} \, , \tag{8}$$

can be rewritten in the form

$$\frac{d\rho}{\rho} = \frac{d\epsilon}{\epsilon f(\epsilon)} - \frac{M}{k_B} \frac{ds}{1+\alpha} \, , \tag{9}$$

where s is the specific entropy and Eqs. (1) and (2) have been used.
To find the density profile at late times, when $P = P_a$ is uniform at
the ambient value, we can integrate (9) along the trajectory of an
element of gas, to obtain

$$\frac{\rho(r,\infty)}{\rho_a} = \exp\left(\int_{\epsilon(r_o,0)}^{\epsilon(r,\infty)} \frac{d\epsilon'}{\epsilon' f(\epsilon')} - \Delta_s \right) \, , \tag{10}$$

where an element of gas at r_o initially moves to r at $t = \infty$, Δ_s is the
integral of the second term in (9), and we have used the fact that
$\rho = \rho_a$ is uniform at $t = 0$. In Eq. (10), the value of $\epsilon(r,\infty)$ is deter-
mined by applying Eq. (1):

$$P_a/\rho(r,\infty) = \epsilon(r,\infty) f\left[\epsilon(r,\infty)\right]. \tag{11}$$

Usually the energy deposition profile $\epsilon(r_o,0)$ is given; it is related
to the initial pressure profile by

$$P(r_o,0)/\rho_a = \epsilon(r_o,0) f\left[\epsilon(r_o,0)\right]. \tag{12}$$

6

Finally, r is related to r_o by integrating the relation

$$\frac{\rho(r_o,0)}{\rho(r,\infty)} = \frac{dr^2}{dr_o^2} \quad,$$

to obtain

$$r_o^2 = \int_o^r dr' \, 2r' \, \rho(r',\infty). \tag{13}$$

Equations (10) - (13), along with the tabulated function $f(\epsilon)$ from Fig. 1, determine the density profile at $t = \infty$, if Δ_s can be specified.

An entropy change occurs only when the outgoing shock wave passes over a particular element of gas. This does not occur at all in the central region of the channel[6], and only once in the outer range of r. Thus

$$\Delta_s = \frac{M}{k_B} \int \frac{ds}{1+\alpha} \quad,$$

where the integral is taken over the shock front, for conditions prevailing when the shock passes over a particular element of gas.

Shock heating typically results in a fairly small change in the final density profile, so a lowest order approximation is given by simply neglecting Δ_s. In Reference 6, we went one step further by giving a heuristic formula for $\Delta_s(r_o)$ for the case of a Bennett heating profile, based on empirical results of fluid code runs with $\gamma = 7/5$, as well as the Rankine-Hugoniot relations and certain other general formal requirements.

The result given there was

$$\exp(\Delta_s) = \frac{\rho-}{\rho+} \left(\frac{6 - \rho-/\rho+}{6\rho-/\rho+ - 1} \right)^{7/5} , \qquad (14)$$

with the ratio of densities downstream and upstream of the shock front given by

$$\frac{\rho-}{\rho+} = \begin{cases} 1 \quad , & r_o/r_B < 0.8 \\[2mm] 1 + 0.33 \left[P(r_o,0)/P_a \right]^{1/4} (r_o/r_B) , & 0.8 < r_o/r_B < 3 \\[2mm] 1 + 1.7 \left[P(r_o,0)/P_a \right]^{1/4} (r_o/r_B) , & 3 < r_o/r_B . \end{cases}$$

We see little hope of writing down any improved closed form for Δ_s that applies to the more complex situation considered here, where γ is no longer constant. However the effect of the shock is merely a small to moderate correction to the density profile at late times, and furthermore the shock effect is greatest in the radial wings, where the gas is not too hot and the assumption that $\gamma = 7/5$ is closer to reality. Thus we shall simply continue to use Eqs. (15) and (16) in Eq. (10) to specify the density profile. As we shall see, the results of this procedure are quite acceptable when compared to fluid code runs.

4. Results

It is most important to use Eq. (1) with the correct dependence $f(\varepsilon)$ to calculate the initial overpressure profile $P(r,0)$ resulting from a given profile $\varepsilon(r,0)$ of energy deposited by the source. As seen in Fig. 1, the pressure can be overestimated by a factor of two or more if the assumption $\gamma = 7/5$, i.e. $f(\varepsilon) = 0.4$, is used to calculate $P(r,0)$. In more familiar terms, the specific heat increases significantly with temperature [but it is more convenient to work with the function $f(\varepsilon)$ defined in Eq. (1), rather than with the specific heat.] The shape as well as the amplitude of the pressure profile is altered; in general, $P(r,0)$ will be broader and more square-shaped than $\varepsilon(r,0)$, as seen in Figs. 2 and 3.

In Figs. 2-9, the gas is taken to be air at standard temperature at pressure before heating by the external source. The energy deposition profile of the external source is taken to be Bennett, i.e. $\varepsilon(r, t = 0) - \varepsilon_a$ has a Bennett shape (where ε_a is the ambient specific energy),

$$\varepsilon(r,t = 0) = \varepsilon_a + \frac{\varepsilon(0,0)}{(1 + r^2/a^2)^2}.$$

Dimensionless units for r and t are used in the figures, $\tilde{r} \equiv r/a$, and $\tilde{t} = c_{sa}t/a$, where c_{sa} is the ambient sound speed. We also use dimensionless units for P and ρ, defined by $\tilde{P} = P/P_a$ and $\rho = \rho/\rho_a$, where P_a and ρ_a are the ambient values. The overpressure factor $\tilde{P}_o$, defined by

$$\tilde{P}_o = \tilde{P}(\tilde{r} = 0, \tilde{t} = 0) - 1,$$

is frequently used to characterize the strength of the initial energy

9

deposition. For the polytropic model which we studied previously, this choice of units reduced the problem to completely dimensionless form; this is not true in the real gas, however, since $f(\varepsilon)$ depends on the specific energy density ε and cannot be scaled out.

In order to examine the effect of real-gas thermodynamics on the hydrodynamic flow subsequent to energy deposition, we shall compare cases in which $\varepsilon(r,0)$ has a Bennett profile, and (i) the assumption $\gamma = 7/5$ is used to calculate $P(r,0)$ and also to treat the subsequent expansion, and the amplitude of $\varepsilon(r,0)$ is such that $\widetilde{P}_o$ has some given value; (ii) the accurate dependence of $f(\varepsilon)$ is used to calculate $P(r,0)$ and also to treat the subsequent expansion, and the amplitude of $\varepsilon(r,0)$ is chosen such that $\widetilde{P}_o$ has the same as in case (i). Case (i) will be referred to as the polytropic case, (ii) as the real gas case.

Figure 4 shows snapshots of the density profile $\rho(r)$ at a series of times, for the real gas case with $P_o = 11.5$. The phenomenology of channel formation -- initial rarefaction wave, deepening and broadening of the channel, shock formation and propagation, density undershoot at late time, and slow return to pressure balance -- is qualitatively similar to that seen with the constant γ assumption.[6] Fig. 5 compares the pressure profile at a particular time for real gas and polytropic cases. We see that the shock is a little stronger for the real gas than for the corresponding polytropic case. To separate the effect of the broadened $P(r,0)$ profile in the real gas case from the effect of the variation of $f(\varepsilon)$ during expansion, we ran another case in

10

which the $P(r,0)$ profile was calculated from the exact thermodynamics, but $f(\varepsilon)$ was set equal to 0.4 during the subsequent expansion. In this case, shown in Fig. 6, the shock was a little weaker for the real gas case. Thus both the change in the $P(r,0)$ profile and the variation of $f(\varepsilon)$ during the subsequent expansion have some influence on the phenomenology (and in opposite directions), but the differences from the ideal-gas case are small, for a given value of $\tilde{P}_o$.

In Figs. 7 and 8, we compare the time dependence of the on-axis density $\rho(0,t)$ for the real gas and polytropic cases. We see that in the polytropic case, the $\rho(0,t)$ curve is smooth, dips slightly below the final equilibrium value and then returns to equilibrium slowly and monotonically[6], but in the real gas case, the channel density exhibits weak oscillations. We have shown in previous work[7] that this type of behavior is characteristic of pressure profiles that are squarer-shaped than Bennett; thus it would appear to be due to the squaring up of the $P(r,0)$ profile that results when the correct $f(\varepsilon)$ is used to calculate $P(r,0)$. However the effect is again small, for practical purposes.

Finally, in Fig. 9, we compare the results of the model developed in Sec. 3, Eqs. (10) - (15) with $\rho(r)$ profiles observed at late times in a code run. We find that the model gives a good representation of the density profile at late times, for all cases that have been run.

5.   Conclusions

It is important to use accurate values of the specific heat, or of the function $f(\varepsilon)$, in calculating the initial pressure profile associated with a given energy deposition source. Changes in the function $f(\varepsilon)$ in air at a few thousand degrees reduce the initial overpressure by about a factor of two, and also make the initial pressure profile considerably squarer-shaped than the energy deposition profile.

However the effect of using accurate values of $f(\varepsilon)$ rather than a constant value $\gamma = 7/5$ during the hydrodynamic expansion is small, with the most noticeable effect being the slight ringing of the on-axis density due to the squarer shape of the $P(r,0)$ profile. For most practical purposes, it is adequate to use $\gamma = 7/5$ during the expansion, provided $P(r,0)$ is calculated accurately. If greater accuracy is needed, it is convenient to formulate the thermodynamic properties of the gas in terms of the function $f(\varepsilon)$, rather than through specific heats or other temperature-dependent quantities. The semi-analytic model of Sec. 3 gives an accurate representation of the density profile of the heated channel at late times, when pressure balance has been restored.

REFERENCES

1. D. A. Miller, L. Baker, J. R. Freeman, L. P. Mix, J. W. Poukey, and T. P. Wright, Proc. 2nd International Topical Conference on High Power Electron and Ion Beam Research and Technology, October 1977, Vol. I, p.393.

2. D. Koopman, J. R. Greig, R. Pechacek, A. Ali, I. M. Vitkovitsky and R. Fensler, Proc. Sixth International Conference on Phenomena in Ionized Gases, Grenoble, France, July 1979, p.C7-419.

3. J. R. Vaill, D. A. Tidman, T. D. Wilkerson, and D. W. Koopman, Appl. Phys. Lett. 17, 20 (1978).

4. R. J. Briggs, T. C. Clark, I. J. Fessenden, R. E. Hester and E. J. Lauer, Proc. 2nd International Topical Conference on High Power Electron and Ion Beam Research and Technology, October 1977, Vol. I, p.319.

5. L. D. Landau and E. M. Lifshitz, Fluid Mechanics (Addison-Wesley, Reading, Massachusetts, 1966, p.393.

6. M. Lampe, H. H. Szu, and S. Kainer, NRL Memo Report 4073 (October 1979).

7. M. Lampe and S. Kainer, NRL Memo Report 4129 (November 1979).

8. J. Boris, Computer Phys. Comm. 12, 16 (1976); NRL Memo Report 3237 (March 1976).

9. D. G. Colombant and J. H. Gardner, J. Comp. Phys. 22, 389 (1976).

10. A. S. Predvoditelev et al, Tables of Thermodynamic Properties of Air (Izdat. Akad. Nauk SSSR, Moscow, 1969. English transl. Associated Technical Services, Inc. Glen Ridge, N.J., 1962).
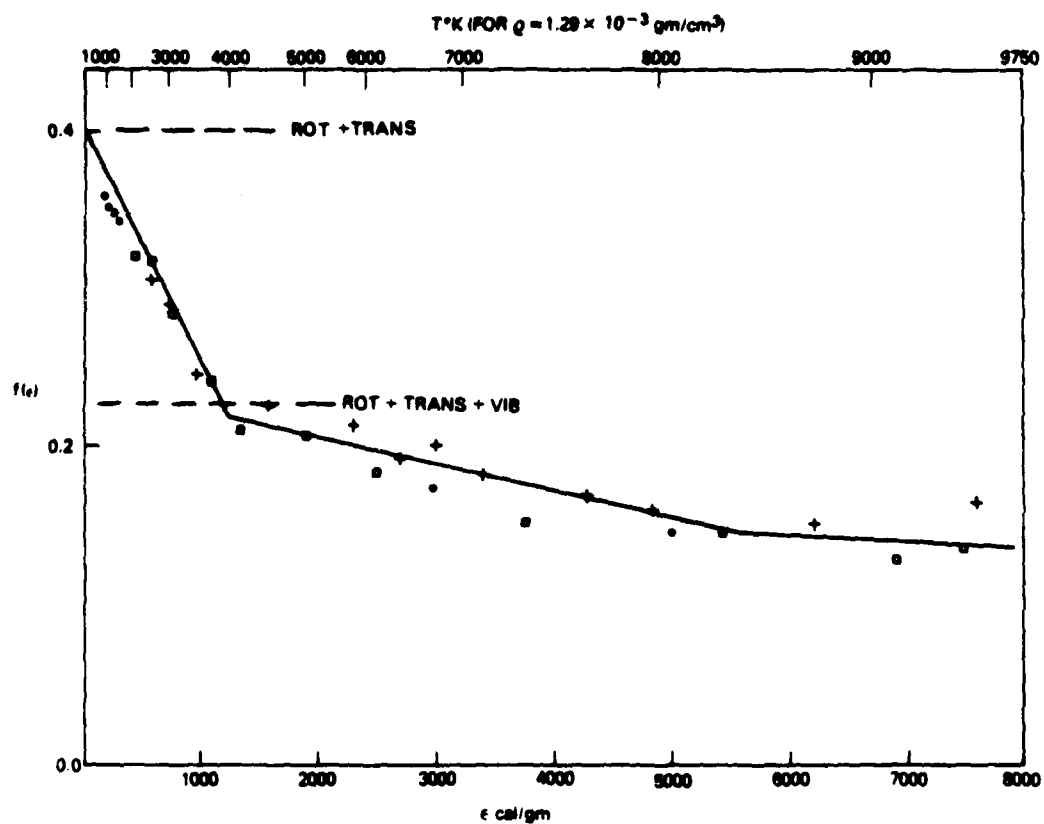
Fig. 1.   Thermodynamic properties of air.   The function f(ε) defined in Eq. (1) is plotted against specific internal energy ε, at various densities: dots correspond to $\rho = 7.0 \times 10^{-5}$ gm/cm^3 (0.054 atm), squares to $\rho = 3.0 \times 10^{-4}$ gm/cm^3 (0.23 atm), crosses to $\rho = 1.29 \times 10^{-3}$ gm/cm^3 (1 atm).
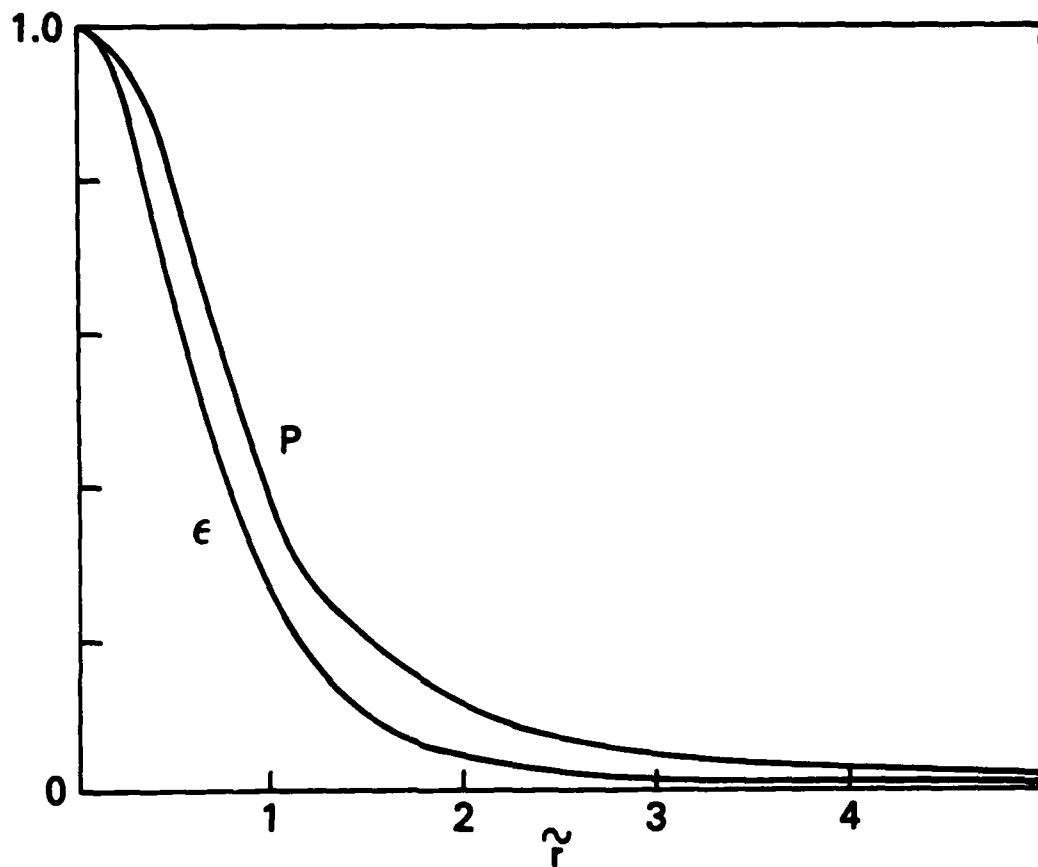
Fig. 2. Energy deposition profile $\varepsilon(r, t = 0)$ and initial pressure
profile $P(r, t = 0)$, each normalized to the value at $r = 0$,
for a case with initial overpressure factor $\tilde{P}_o = 46$. The
two curves differ only because of the deviation of the real
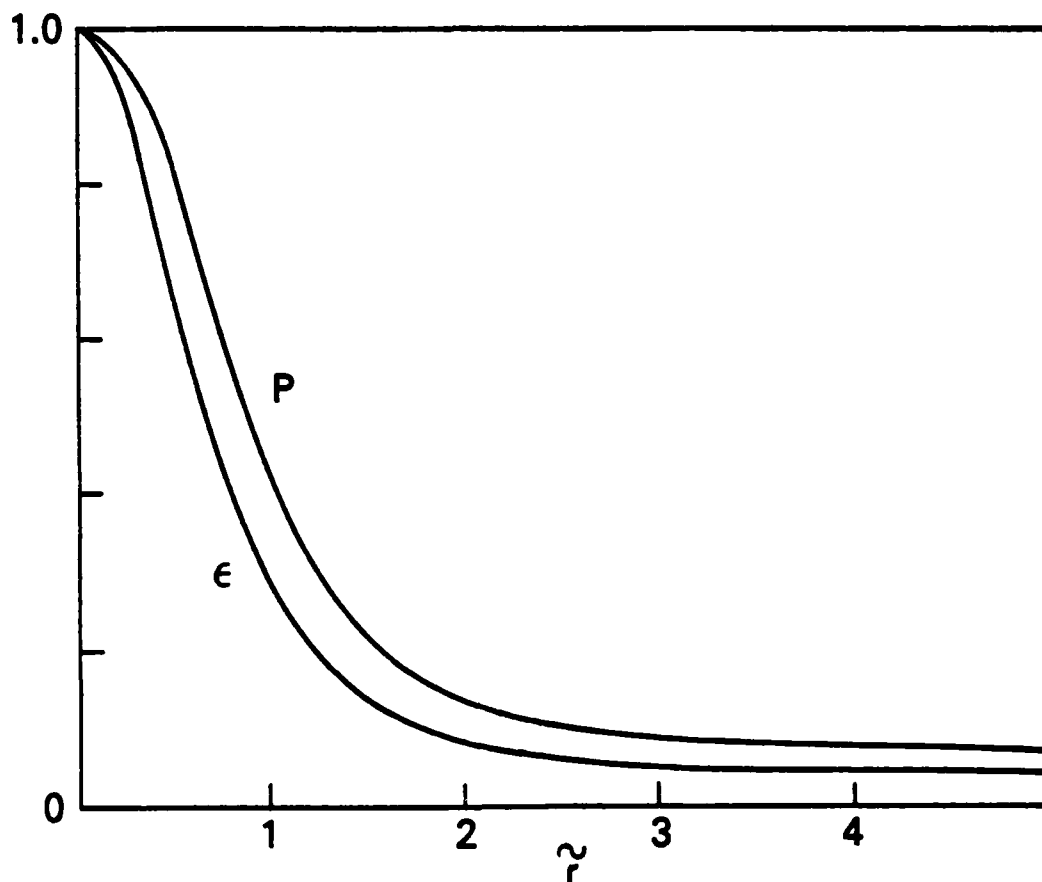gas from polytropic, i.e. the variation of $f(\varepsilon)$.

Fig. 3. Energy deposition profile $\varepsilon(r, t = 0)$ and initial pressure profile $P(r, t = 0)$, each normalized to the value at $r = 0$, for a case with initial overpressure factor $\widetilde{P}_o = 11.5$. The two curves differ only because of the deviation of the real gas from polytropic, i.e. the variation of $f(\varepsilon)$.
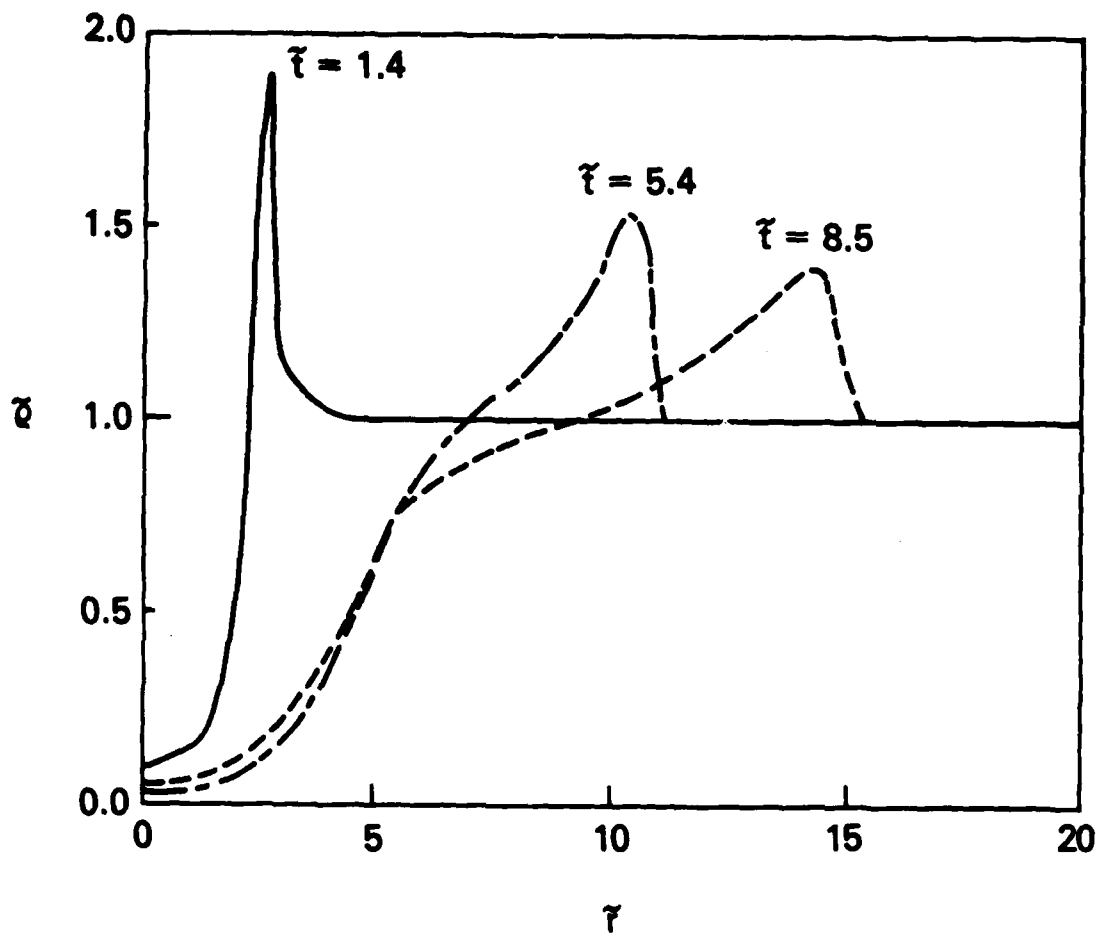
Fig. 4. Radial density profile in a real gas at various times. The energy deposition profile $\varepsilon(r, t = 0)$ is Bennett, and corresponds to an overpressure factor $\widetilde{P}_o = 11.5$.
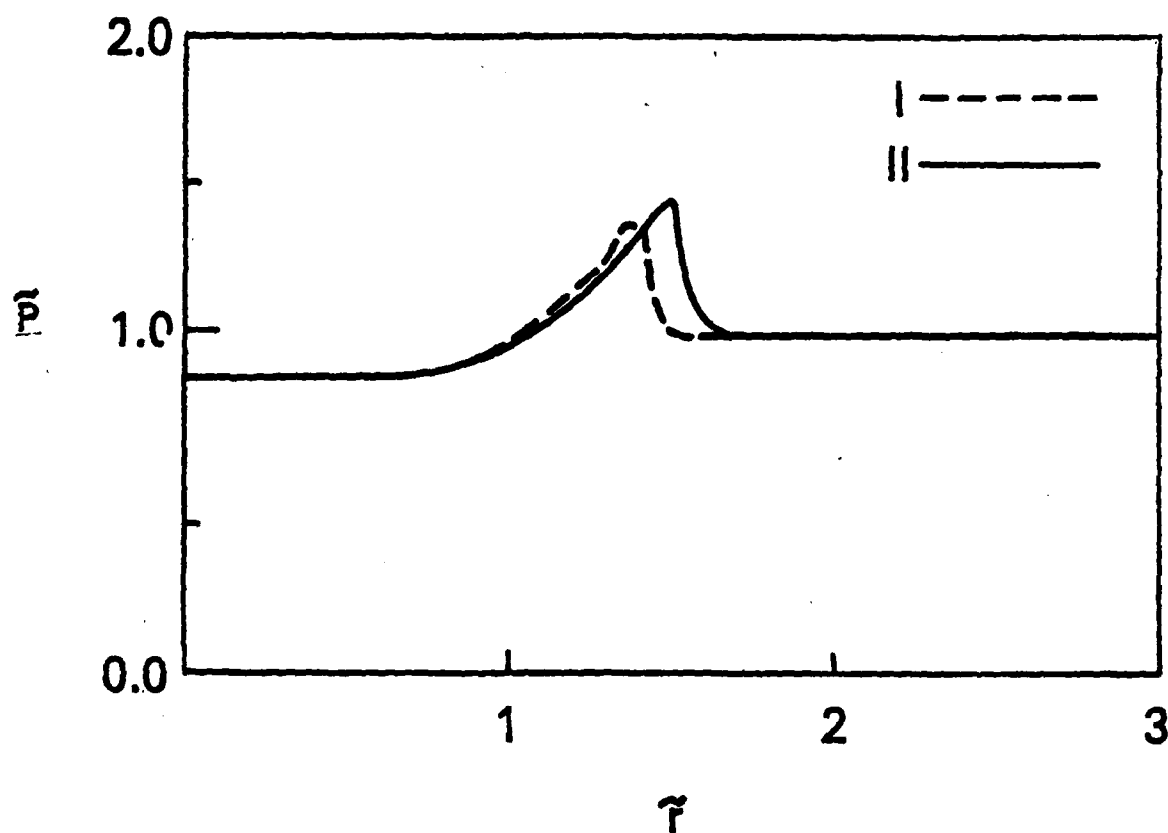
Fig. 5. Radial pressure profile at $\widetilde{t} = 9.0$, for a case with $\widetilde{P}_o = 26.1$.
Curve I: ideal gas, $\gamma = 7/5$. Curve II: real gas.
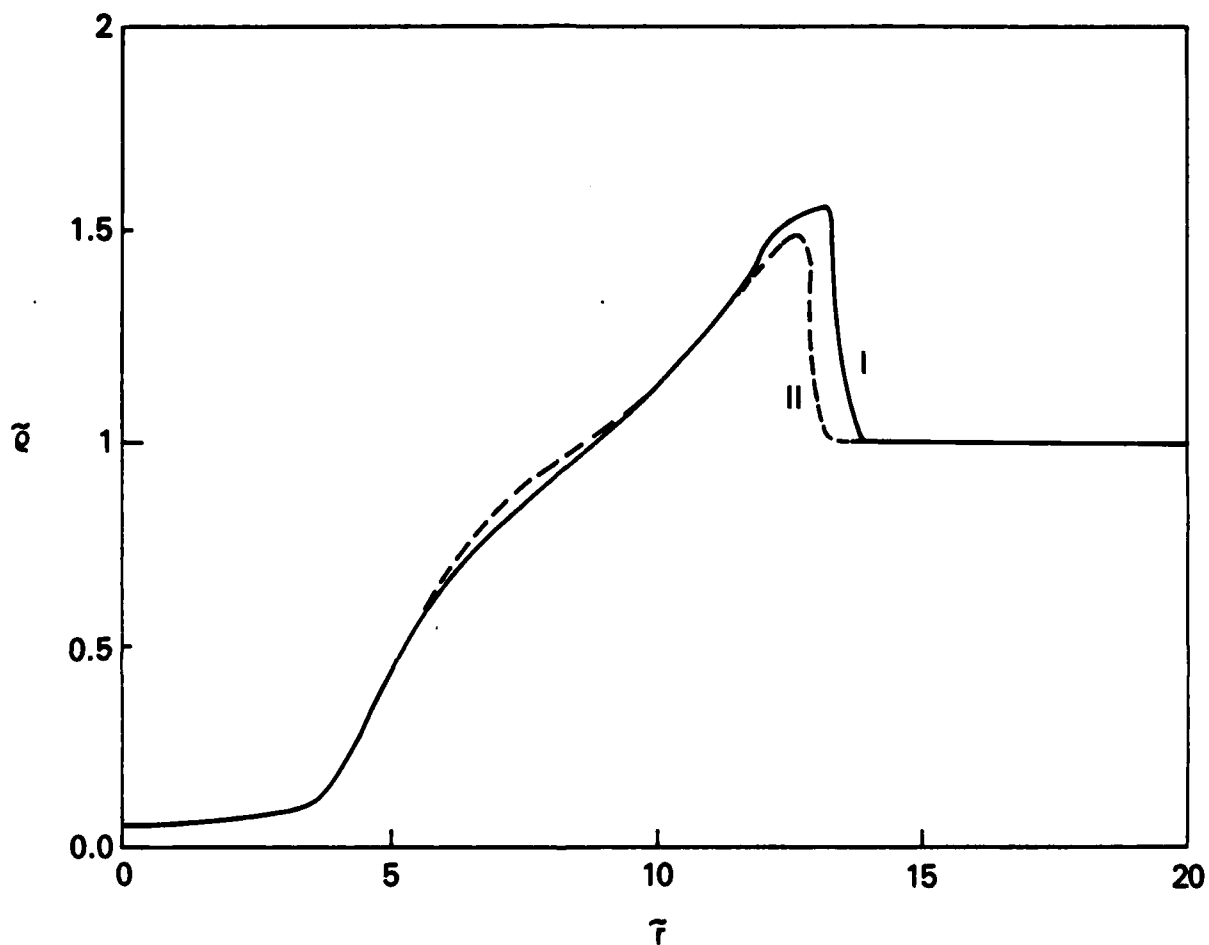
Fig. 6. Radial density profile at $\tilde{t}$ = 6.33 for two cases with $\tilde{P}_o$ = 26.1 and Bennett energy deposition profile. In each case, the initial pressure profile $P(r,0)$ is calculated using the real gas function $f(\varepsilon)$. For Curve I, the polytropic model with $\gamma = 7/5$ is used to treat the subsequent expansion; for Curve II, the real gas properties are used.

19

Fig. 7. Time evolution of $\tilde{\rho}(\tilde{r} = 0)$ for Bennett deposition profile, initial overpressure factor $\tilde{P}_o$ = 26.1, in real gas.

20

Fig. 8. Time evolution of $\tilde{\rho}\,(\tilde{r} = 0)$ for Bennett deposition profile, initial overpressure factor $\tilde{P}_o = 26.1$, in polytropic gas.
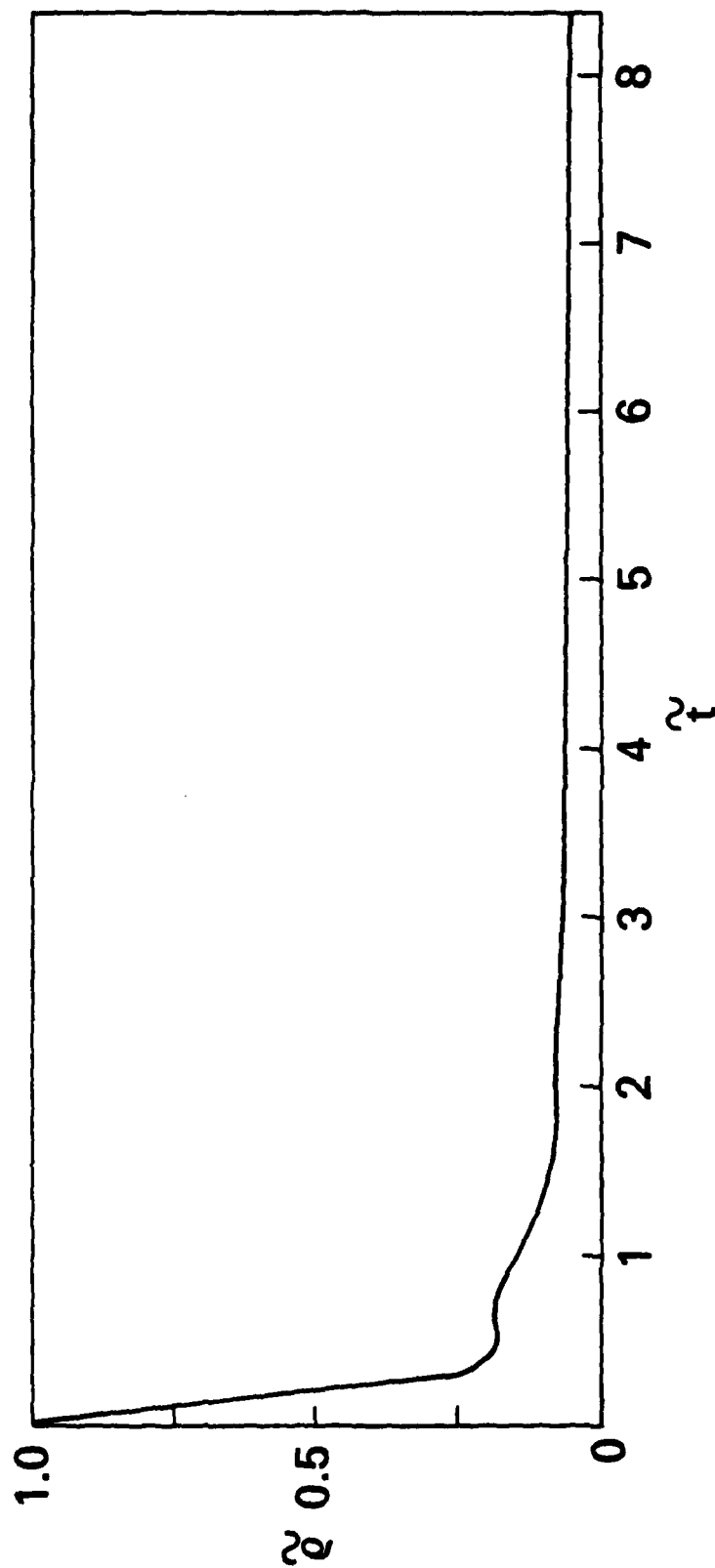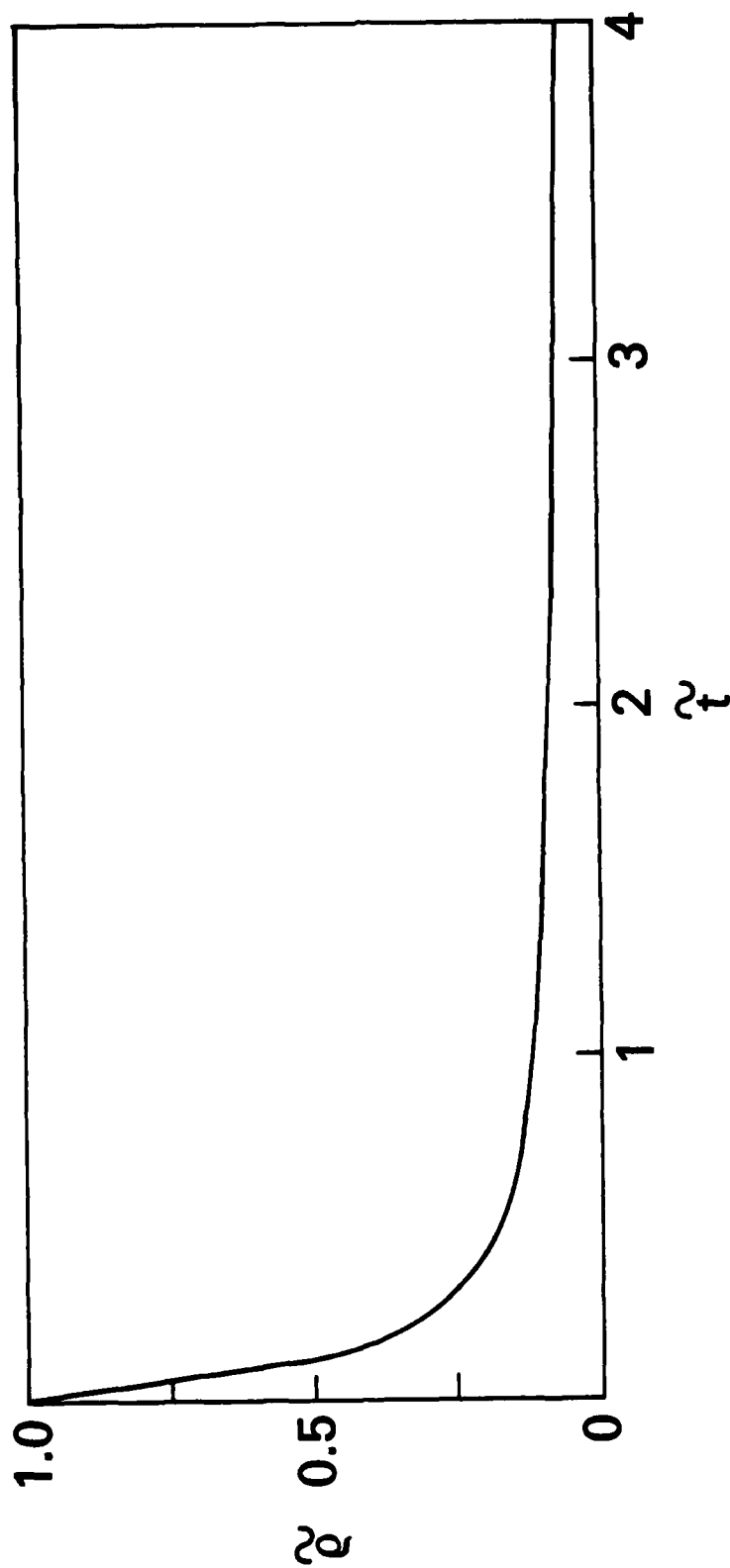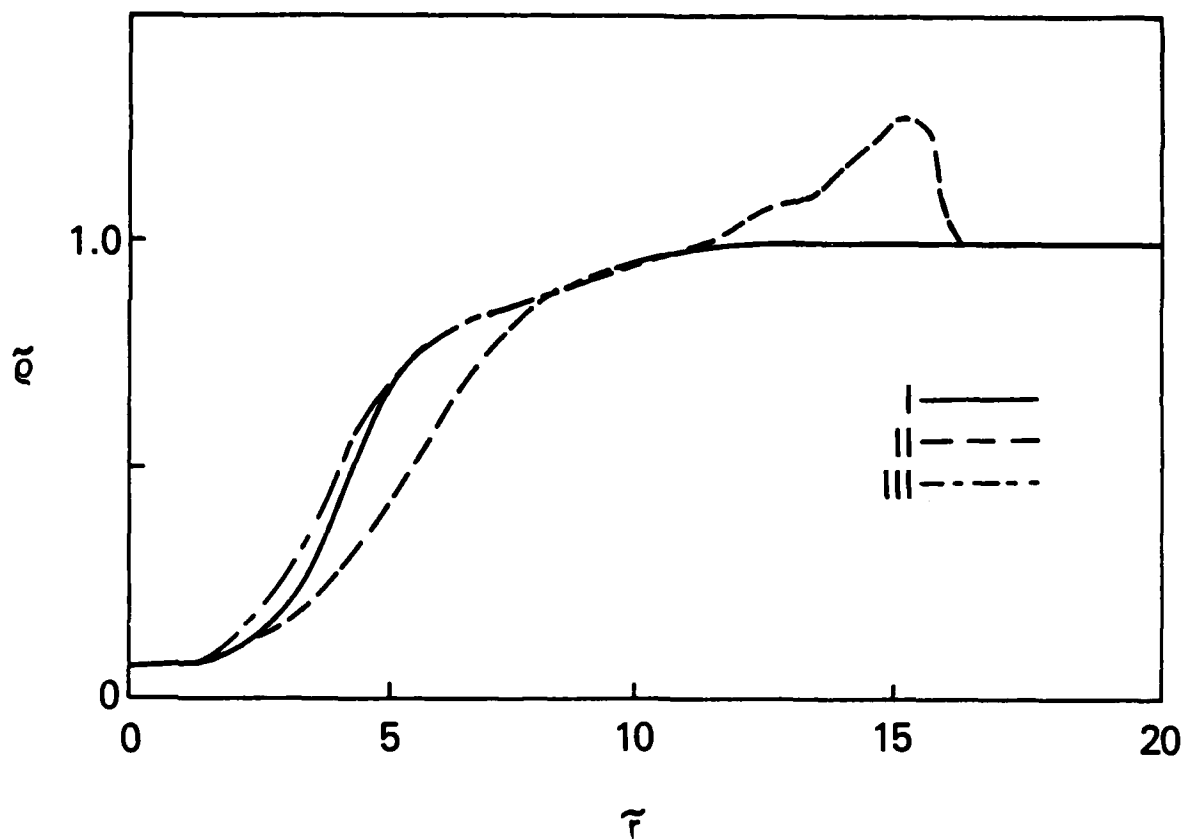
Fig. 9. Radial density profiles at late times in real gas. Curve I: analytic solution. Curve II: hydrodynamic code solution at $\tilde{t} = 9.66$. Curve III: hydro code solution at $\tilde{t} = 18.0$. The initial overpressure factor was $\tilde{P}_o = 11.5$.

DISTRIBUTION LIST

1. Commander
   Naval Sea Systems Command
   Department of the Navy
   Washington, D.C. 20363
      Attn: NAVSEA 03H (Dr. C. F. Sharn)

2. Central Intelligence Agency
   P. O. Box 1925
   Washington, D.C. 20013
      Attn: Dr. C. Miller/OSI

3. Air Force Weapons Laboratory
   Kirtland Air Force Base
   Albuquerque, New Mexico 87117
      Attn: Lt. Col. J. H. Havey

4. U. S. Army Ballistics Research Laboratory
   Aberdeen Proving Ground, Maryland 21005
      Attn: Dr. D. Eccleshall (DRXBR-BM)

5. Ballistic Missile Defense Advanced Technology Center
   P. O. Box 1500
   Huntsville, Alabama 35807
      Attn: Dr. L. Havard (BMDSATC-1)

6. B-K Dynamics, Inc.
   15825 Shady Grove Road
   Rockville, Maryland 20850
      Attn: Mr. I. Kuhn

7. Intelcom Rad Tech
   P. O. Box 81087
   San Diego, California 92138
      Attn: Mr. W. Selph

8. Lawrence Livermore Laboratory
   University of California
   Livermore, California 94550
      Attn: Dr. R. J. Briggs
            Dr. T. Fessenden
            Dr. E. P. Lee

9. Mission Research Corporation
   735 State Street
   Santa Barbara, California 93102
      Attn: Dr. C. Longmire
            Dr. N. Carron

10. National Bureau of Standards
    Gaithersburg, Maryland 20760
        Attn: Dr. Mark Wilson

11. Science Applications, Inc.
    1200 Prospect Street
    La Jolla, California 92037
        Attn: Dr. M. P. Fricke
               Dr. W. A. Woolson

12. Science Applications, Inc.
    Security Office
    5 Palo Alto Square, Suite 200
    Palo Alto, California 94304
        Attn: Dr. R. R. Johnston
              Dr. Leon Feinstein

13. Science Applications, Inc.
    1651 Old Meadow Road
    McLean, Virginia 22101
        Attn: Mr. W. Chadsey

14. Science Applications, Inc.
    8201 Capwell Drive
    Oakland, California 94621
        Attn: Dr. J. E. Reaugh

15. Naval Surface Weapons Center
    White Oak Laboratory
    Silver Spring, Maryland 20910
        Attn: Mr. R. J. Biegalski
               Dr. R. Cawley
               Dr. J. W. Forbes
               Dr. D. L. Love
               Dr. C. M. Huddleston
               Dr. G. E. Hudson
               Mr. W. M. Hinckley
               Mr. G. J. Peters
               Mr. N. E. Scofield
               Dr. E. C. Whitman
               Dr. M. H. Cha
               Dr. H. S. Uhm
               Dr. R. Fiorito

16. C. S. Draper Laboratories
    Cambridge, Massachusetts 02139
        Attn: Dr. E. Olsson
               Dr. L. Matson

17. M.I.T. Lincoln Laboratories
    P. O. Box 73
    Lexington, Massachusetts 02173
        Attn: Dr. J. Salah

18. Physical Dynamics, Inc.
    P. O. Box 1883
    La Jolla, California 92038
       Attn: Dr. K. Brueckner

19. Office of Naval Research
    Department of the Navy
    Arlington, Virginia 22217
       Attn: Dr. W. J. Condell (Code 421)

20. Avco Everett Research Laboratory
    2385 Revere Beach Pkwy.
    Everett, Massachusetts 02149
       Attn: Dr. R. Patrick
             Dr. Dennis Reilly

21. Defense Technical Information Center
    Cameron Station
    5010 Duke Street
    Alexandria, VA 22314 (12 copies)

22. Naval Research Laboratory
    Washington, D.C. 20375

                M. Lampe - Code 4792 (50 copies)
                M. Friedman - Code 4700.1
                J. R. Greig - Code 4763
                I. M. Vitkovitsky - Code 4770
                J. B. Aviles - Code 4665
                M. Haftel - Code 4665
                T. Coffey - Code 4000
                Superintendent, Plasma Physics Div. - Code 4700 (25 copies)
                Branch Head, Plasma Theory Branch - Code 4790
                Library - Code 2628
                A. Ali - Code 4700.1
                D. Book - Code 4040
                J. Boris - Code 4040
                I. Haber - Code 4790
                S. Kainer - Code 4790
                A. Robson - Code 4760
                P. Sprangle - Code 4790
                D. Colombant - Code 4790
                M. Picone - Code 4040
                D. Spicer - Code 4169
                M. Raleigh - Code 4760
                R. Pechacek - Code 4763

23. Defense Advanced Research Projects Agency
    1400 Wilson Blvd.
    Arlington, VA 22209
        Attn: Dr. J. Mangano
               Dr. J. Bayless

24. JAYCOR
    205 S. Whiting St.
    Alexandria, VA 22304
        Attn: Drs. D. Tidman
                    R. Hubbard
                    J. Guillery

25. JAYCOR
    Naval Research Laboratory
    Washington, D.C. 20375
        Attn: Dr. R. Fernsler - Code 4770
               Dr. G. Joyce - Code 4790
               Dr. S. Goldstein - 4770

26. SAI
    Naval Research Laboratory
    Washington, D.C. 20375
        Attn: A. Drobot - Code 4790
               W. Sharp - Code 4790

27. Physics International, Inc.
    2700 Merced Street
    San Leandro, CA.
        Attn: Drs. S. Putnam
                    E. Goldman

28. Mission Research Corp.
    1400 San Mateo, S.E.
    Albuquerque, NM   87108
        Attn: Dr. Brendan Godfrey

29. Princeton University
    Plasma Physics Laboratory
    Princeton, NJ 08540
        Attn: Dr. Francis Perkins, Jr.

30. McDonnell Douglas Research Laboratories
    Dept. 223, Bldg. 33, Level 45
    Box 516
    St. Louis, MO 63166
        Attn: Dr. Michael Greenspan

31. Cornell University
    Ithaca, NY 14853
      Attn: Prof. David Hammer

32. Sandia Laboratories
    Albuquerque, NM 87185
      Attn: Dr. Bruce Miller
             Dr. Barbara Epstein

33. University of California
    Physics Department
    Irvine, CA 92717
      Attn: Dr. Gregory Benford

34. Defense Technical Information Center
    Cameron Station
    5010 Duke Street
    Alexandria, VA 22314 (12 copies)

35. Beers Associates Inc.
    Attn: Dr. Douglas Strickland
    P. O. Box 2549
    Reston, Va. 22090